Available online at www.sciencedirect.com
SCIENCE DIRECT®
Earth and Planetary Science Letters 237 (2005) 135–155
EPSL
www.elsevier.com/locate/epsl

$^{231}Pa/^{230}Th$ fractionation by ocean transport, biogenic particle flux and particle type

Mark Siddall [a,*], Gideon M. Henderson [b], Neil R. Edwards [c], Martin Frank [d,1], Simon A. Müller [a], Thomas F. Stocker [a], Fortunat Joos [a]

[a] *Climate and Environmental Physics, Physics Institute, University of Bern, Bern, Switzerland*
[b] *Department of Earth Sciences, Oxford University, Parks Road, Oxford, United Kingdom*
[c] *Open University, Milton Keynes, United Kingdom*
[d] *Institute for Isotope Geology and Mineral Resources Department of Earth Sciences, ETH, Zurich, Switzerland*

Received 28 January 2005; received in revised form 17 May 2005; accepted 25 May 2005
Available online 19 July 2005
Editor: H. Elderfield

Abstract

^{231}Pa and ^{230}Th are removed from the water column by a process of reversible scavenging which quickly removes ^{230}Th to the sediment. ^{231}Pa is less efficiently scavenged onto particles than ^{230}Th and is therefore more effectively transported via advection and diffusion before it reaches the ocean sediment. This study combines particle fields (dust, opal, $CaCO_3$, POC) derived from observations with the Bern3D intermediate complexity ocean model and an equilibrium-scavenging model for isotopes. The equilibrium partition coefficient for particulate versus dissolved isotope activity is varied with particle type. The model can explain many of the features of the global ^{231}Pa and ^{230}Th distribution. The success of such a simple model at representing the global pattern of $^{231}Pa/^{230}Th$ activity ratio supports the use of this proxy in paleoceanographic studies. We use the model to address the controversy concerning which particle types are dominant in fractionating $^{231}Pa/^{230}Th$ in the ocean. The lithogenic (dust) flux is found to be unimportant for $^{231}Pa/^{230}Th$ fractionation— the ocean fractionation of $^{231}Pa/^{230}Th$ is dominated by the distribution of the $CaCO_3$ and opal flux. We also confirm that opal is a weak scavenger of ^{230}Th.

Keywords: ^{230}Th; ^{231}Pa; scavenging; meridional overturning circulation; particles; paleoceanography

1. Introduction

^{231}Pa (32.5 kyr half-life) and ^{230}Th (75.2 kyr half-life) are formed by the α decay of ^{235}U and ^{234}U, respectively. Because the activity of U in the ocean is uniform [1] ^{231}Pa and ^{230}Th are produced at a constant rate with a production activity ratio (β^{Pa}/β^{Th}) of

* Corresponding author. Tel.: +41 31 631 44 64; fax: +41 31 631 87 42.
E-mail address: siddall@climate.unibe.ch (M. Siddall).
[1] Now at IFM-GEOMAR, Leibniz Institute for Marine Sciences, University of Kiel, Wischhofstrasse 1–3, 24148 Kiel, Germany.

0012-821X/$ - see front matter © 2005 Elsevier B.V. All rights reserved.
doi:10.1016/j.epsl.2005.05.031

0.093 throughout the ocean (see Table 1 for a list of constants). In other words there is a uniform, steady source of ^{231}Pa and ^{230}Th at every point in the ocean.

Dissolved ^{231}Pa and ^{230}Th are removed from the water column through reversible scavenging by falling particles considerably more rapidly than by the radio-decay of either isotope [2,3]. Reversible scavenging is the process of isotope adsorption onto particles with subsequent desorption due to the release of the isotope during dissolution, particle aggregation/disagregation, or variation in the dissolved isotope concentration [4]. Reversible scavenging causes the activities of ^{230}Th and ^{231}Pa to generally increase with water depth in both the particulate and dissolved form [2,5].

Differential scavenging of ^{231}Pa and ^{230}Th in the water column means that ^{230}Th is removed more readily from solution than ^{231}Pa. Less efficient scavenging of dissolved ^{231}Pa gives it an ocean residence time of approximately 200 years while that of dissolved ^{230}Th is approximately 30 years [6]. Because of its longer residence time, ^{231}Pa is more strongly advected by ocean circulation than ^{230}Th, making the sediment $^{231}Pa_{xs}/^{230}Th_{xs}$ an important measure of ocean circulation [6,7] (the xs subscript is used to indicate that the values are for excess ^{231}Pa and ^{230}Th activities, corrected for ^{231}Pa and ^{230}Th isotopes supported by U decay). In the absence of ocean advection and mixing ^{231}Pa and ^{230}Th would be removed from the water column at a fixed ratio identical to the production ratio. Consequently the sediment $^{231}Pa_{xs}/^{230}Th_{xs}$ would equal the production ratio everywhere in the world ocean [2].

Advection of ^{231}Pa in the Atlantic depends on the strength of the Atlantic meridional overturning circulation (AMOC) [6,7]. Recent work on sediment

Table 1
List of abbreviations and values for various parameters used in text

Variable	Symbol	Control run	Sensitivity tests	Units
Isotope variables				
^{231}Pa production from U decay	β^{Pa}	2.33×10^{-3}	–	dpm m^{-3} yr^{-1}
^{230}Th production from U decay	β^{Th}	2.52×10^{-2}	–	dpm m^{-3} yr^{-1}
^{231}Pa decay constant	λ^{Pa}	2.13×10^{-5}	–	yr^{-1}
^{230}Th decay constant	λ^{Th}	9.22×10^{-6}	–	yr^{-1}
Particle associated activity	A_p	–	–	dpm m^{-3} yr^{-1}
Dissolved activity	A_d	–	–	dpm m^{-3} yr^{-1}
Bulk particle activity	A_b	–	–	dpm m^{-3} yr^{-1}
Total particle activity	A_{total}	–	–	dpm m^{-3} yr^{-1}
Particle flux variables				
Penetration depth for $CaCO_3$	z_p	2000	1000, 3000	m
Dissolution constant for POC	ε	0.858	0.658, 1.058	–
Thickness of eutrophic layer	z_0	–	–	m
Average particle sinking velocity	w_s	1000	500, 1500	M yr^{-1}
Ocean temperature	T	–	–	°C
Particle flux from surface	F	–	–	mol C yr^{-1}
Dimensionless part. conc.	C	–	–	–
K values				
Equilibrium partition coefficient:	K_{ref}	10^7	10^6, 10^9	
^{230}Th scavenging by $CaCO_3$	K^{Th}_{car}	K_{ref}	$K_{ref}/49$, K_{ref}	–
^{230}Th scavenging by opal	K^{Th}_{opal}	$K_{ref}/20$	$K_{ref}/49$	–
^{230}Th scavenging by POC	K^{Th}_{POC}	K_{ref}	$K_{ref}/49$	–
^{230}Th scavenging by dust	K^{Th}_{dust}	0	$10\times K_{ref}$	–
^{231}Pa scavenging by $CaCO_3$	K^{Pa}_{car}	$K_{ref}/40$	$K_{ref}/49$, K_{ref}	–
^{231}Pa scavenging by opal	K^{Pa}_{opal}	$K_{ref}/6$	$K_{ref}/4.9$, $K_{ref}/49$, K_{ref}	–
^{231}Pa scavenging by POC	K^{Pa}_{POC}	K_{ref}	$K_{ref}/49$	–
^{231}Pa scavenging by dust	K^{Pa}_{dust}	0	K_{ref}	–

K values for the control run are adapted from Chase et al. [10]. K values for sensitivity experiments are based on Luo and Ku [11,13,14].

$^{231}Pa_{xs}/^{230}Th_{xs}$ from the Bermuda Rise has found values approaching the production ratio during the coldest interval during deglaciation in the North Atlantic region [8]. Such $^{231}Pa_{xs}/^{230}Th_{xs}$ values suggest that the AMOC may have approached stagnation over this period [8], assuming that changes in the $^{231}Pa_{xs}/^{230}Th_{xs}$ at one site are representative of changes in the zonally integrated circulation.

1.1. Observations of ^{231}Pa and ^{230}Th partition coefficients

If one assumes that the rate of adsorption and desorption are fast compared with the rate of removal of particulates the partition of ^{230}Th activity between dissolved and particle-associated phases will be in equilibrium [2]. In the open ocean this is a reasonable assumption [9]. The ratio between dissolved, A_d, and particle-associated, A_p, activity is given by a dimensionless equilibrium partition coefficient, K,

$$K_p^i = \frac{A_p^i}{A_d^i C_p}, \quad (1)$$

where C_p is the dimensionless ratio of the particle mass per cubic m to the density of the fluid and the isotope activities are in units of dpm m^{-3}. The superscript i represents ^{231}Pa or ^{230}Th and the subscript p represents the particle type (Particulate Organic Carbon (POC), dust, $CaCO_3$ or opal). The term A_b used later in the text refers to the bulk, or total activity associated with particles.

Chase et al. [10] and Luo and Ku [11] have found that the values of the equilibrium ^{231}Pa and ^{230}Th partition coefficients for the total or bulk particle flux (K_{bulk} values) depend on the percentage concentrations of opal, $CaCO_3$, POC and lithogenic particles, although these authors are in disagreement over which particles drive changes in the equilibrium values [10–14]. Chase et al. [10] find that opal preferentially scavenges ^{231}Pa while $CaCO_3$ preferentially scavenges ^{230}Th. Lithogenic particles are typically at least an order of magnitude less prevalent in the open ocean than biogenic particles (Fig. 1) and may therefore be expected to be less significant scavengers of ^{231}Pa and ^{230}Th than biogenic particles [10]. Luo and Ku [11], however, find that the equilibrium partition coefficients of ^{230}Th and ^{231}Pa for lithogenic particles are respectively

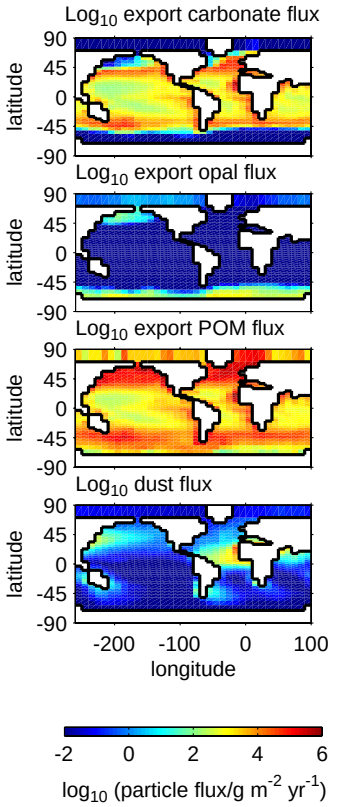

Fig. 1. Surface particle fluxes interpolated to the model grid and used to force the model. Particle flux is given in g m^{-2} yr^{-1} on a $\log_{10}$ colour scale. Details of the derivation of particle surface forcing fields are given in the text. All values are annual averages.

490 and 45 times stronger than those for biogenic particles (POC, opal, $CaCO_3$) so that despite the low concentration of lithogenic particles in the ocean they may still be important scavengers of ^{231}Pa and ^{230}Th. It must be noted that Luo and Ku [11,13,14] estimate such high equilibrium partition coefficients for lithogenic particles (unprecedented before Luo and Ku [11]) by extrapolating from bulk particle samples with only ~5% lithogenic material.

Before the dependence of $^{231}Pa/^{230}Th$ fractionation by different particles is fully understood it is not possible to use the sediment $^{231}Pa_{xs}/^{230}Th_{xs}$ as a simple proxy for ocean advection. Resolving the controversy concerning $^{231}Pa/^{230}Th$ fractionation by lithogenic versus biogenic particles is an important step towards understanding changes in ocean advection in the past using the sediment $^{231}Pa_{xs}/^{230}Th_{xs}$ record.

1.2. Previous modelling of ^{231}Pa / ^{230}Th

Using a zonally averaged, circulation-biogeochemistry model, Marchal et al. [7] applied the reversible scavenging model of Bacon and Anderson [2] to ^{231}Pa and ^{230}Th. In that work ^{231}Pa was scavenged ten times more effectively by biogenic opal than by POC or $CaCO_3$. Marchal et al. [7] kept desorption rate constants for ^{231}Pa and ^{230}Th fixed at a single value throughout the model for all particle types in a fashion which does not allow for the effects of the dissolution of different particle types on desorption of ^{231}Pa and ^{230}Th. The adsorption/desorption model of Marchal et al. [7] does, however, represent other factors involved in desorption (such as particle disaggregation). Although the biogeochemistry component of the model was used to calculate fields of POC and $CaCO_3$, the flux of biogenic opal in the Southern Ocean was prescribed. The Marchal et al. [7] model can approximate well the latitudinal and depth variations in ^{231}Pa and ^{230}Th and supports the notion that preferential adsorption of ^{231}Pa by opal in the Southern Ocean leads to high ^{231}Pa/^{230}Th ratios there. Ocean circulation is, however, characterised by important east–west gradients and so there are clear limitations in using a zonally averaged model. The North Atlantic is key in determining the sensitivity of ^{231}Pa and ^{230}Th distributions to changes in the AMOC and needs to be well represented but there are significant differences in the particle flux and ocean circulation between the east and west of the basin that cannot be accounted for in a zonally averaged model. The equatorial Pacific also has pronounced east–west variation in particle flux. To account for these effects an obvious step forward is the use of a 3-dimensional ocean model.

A 3-dimensional model has been used by Henderson et al. [9] to model the ocean ^{230}Th. They used the Hamburg Large Scale Geostrophic Ocean Circulation Model to obtain an estimate of the ocean circulation and the Hamburg Oceanic Carbon Cycle Model to estimate ocean particle fluxes. They restricted their study to ^{230}Th and assumed a particle-concentration dependent equilibrium partition coefficient [15,4]. Unlike Marchal et al. [7], the Henderson et al. [9] approach allows for separate 'desorption' effects due to both equilibrium scavenging and particle dissolution. Different particle types dissolve differently with respect to depth, temperature and other factors. Given the preferential scavenging effects of different particle types [11,10] this differential dissolution is likely to be important when considering the 3-dimensional distribution of ^{231}Pa and ^{230}Th in the ocean.

Apart from dissolution effects the Marchal et al. [7] and Henderson et al. [9] approaches are equivalent as long as the rates of adsorption and desorption prescribed by Marchal et al. [7] are fast compared with the rate of removal of the particulate matter, as is the case in the open ocean [2]. The Henderson et al. [9] approach did not consider ^{231}Pa but it makes use of equilibrium ^{230}Th partition coefficients and is well suited to making use of recently observed relative scavenging equilibria with respect to different particle types [11,10]. For this reason it is the favoured approach in this paper although here we include representation of ^{231}Pa. An added advantage of this approach is that, because a partition coefficient is prescribed, it involves the use of only one ocean tracer per isotope (the total activity of the isotope), as opposed to the two tracers needed in Marchal et al. [7] (the dissolved and particulate activities of each isotope).

By studying the behaviour of ^{231}Pa and ^{230}Th in the Bern3D intermediate complexity ocean model this paper is a step towards enabling a more rigorous understanding of the relationship between the 2-dimensional ocean sediment $^{231}Pa_{xs}/^{230}Th_{xs}$ and the 3-dimensional paleocean circulation. Thus we extend the work of Marchal et al. [7] to include the effects of particulate dissolution; 3-dimensional ocean circulation; and particle fields for dust, opal, POC and $CaCO_3$. Particular emphasis is placed on resolving the disagreement over the importance of ^{231}Pa and ^{230}Th scavenging by lithogenic particles [10,12–14].

2. Method

2.1. The ocean model

The ocean circulation used for this work is given by the Bern3D model [16]. The Bern3D model is a computationally efficient ocean model of intermediate complexity based on the planetary geostrophic

equations complemented by a linear drag term [17]. Efficiency is a result of low horizontal resolution, 36 by 36 cells, and simplified physics. Ocean tracers are subject to advection by the velocity field, diffusion and convection. Simplified physics implies that model diffusion represents a larger range of processes than in more complex models. The two 'active' tracers, temperature and salinity, which define the density and hence the velocity, are treated exactly analagously to the passive tracers (i.e., tracers which do not affect the circulation), such as ^{231}Pa and ^{230}Th. In relation to the ocean model of [17], the present model differs principally in using seasonally varying forcing and higher vertical resolution, with 32 levels instead of 8. The convection and time stepping schemes and the eddy-induced advection have also been improved [16].

To derive the circulation state the model equations are integrated forward in time for around 5000 years by which time annually averaged tracer fields and velocities are almost exactly steady. The steadily oscillating final state can generally be assumed to be insensitive to the initial conditions and thus dependent essentially on the forcing fields for temperature and salinity [18], as well as wind stress [19] applied at the surface boundary layer.

Model parameters have been tuned such that this steadily oscillating state provides a solution that closely matches measured values for radiocarbon in the preindustrial North Atlantic, North Pacific and Southern Ocean as well as chlorofluorocarbon inventories for the Indopacific and the Southern Ocean [20]. These ocean tracers are chosen to represent a variety of ventilation timescales ranging from years to centuries. This state can thus be taken to represent relatively steady pre-industrial oceanic conditions. Full details of the model and its tuning as used for this work are described in Müller et al. [16]. All results presented are annual averages for the steadily oscillating state.

2.2. Particle fields

To generate surface particle fluxes, the export production of POC was estimated using the model of Laws et al. [21], which calculates the ratio of total primary production to export production (the export production ratio) from the total primary production and ocean temperature. Primary production was provided by the Vertically Generalised Production Model (VGPM) of Behrenfield and Falkowski [22] and mean temperatures for the upper 200 m of the ocean were used [18]. Sampling of the data fields onto the model grid was carried out by taking the average values from the data points within each model grid cell. The export production of POC was then calculated using the annual mean total primary production from the VGPM of Behrenfield and Falkowski [22] and the derived export production ratio. To generate the export production of $CaCO_3$ and biogenic opal algorithms similar to those described by Maier–Reimer [23] were used. The potential particle flux due to the production of biogenic opal P_{opal}, is defined as:

$$P_{\mathrm{opal}} = r_{\mathrm{opal}} \int_{z=200}^{z=0} R \frac{[Si]^2}{[Si] + [Si_0]} \cdot z, \tag{2}$$

where z is depth. $[Si(z)]$ is the silicic acid concentration in mol m^{-3} [24], r_{opal} is the observed dissolution/production ratio for biogenic opal of 0.5 in the high latitudes [25] and $[Si_0]$ is set to 0.004 mol m^{-3}. R relates to the maximum rate of uptake of silicic acid and is set at 0.015 yr^{-1}. Following Heinze [26], the potential particle flux due to the formation of carbonate shells, P_{car}, is given as

$$P_{\mathrm{car}} = r_{\mathrm{car}} P \frac{c_1 \exp(c_2(T_{\mathrm{Lev}} - T_{\mathrm{r}}))}{1 + c_1 \exp(c_2(T_{\mathrm{Lev}} - T_{\mathrm{r}}))}, \tag{3}$$

where T_{Lev} is the mean temperature for the top 200 m [18], P is the export flux, r_{car} is the maximum value of the production ratio of carbonate to total flux that would occur in warm waters and c_1 and c_2 are parameters. After Marchal et al. [27], T_{r} was set to 10 °C, $c_1 = 1$, $c_2 = 0.6$ °C^{-1} and $r_{\mathrm{car}} = 0.096$. The potential fluxes P_{opal} and P_{car} may then be combined to give the actual opal (F_{opal}) and carbonate (F_{car}) fluxes from the surface layer in mol m^{-2} yr^{-1} [23]

$$F_{\mathrm{opal}} = \frac{P_{\mathrm{opal}}^2}{P_{\mathrm{opal}} + P_{\mathrm{car}}}, \tag{4}$$

$$F_{\mathrm{car}} = \frac{P_{\mathrm{car}}^2}{P_{\mathrm{opal}} + P_{\mathrm{car}}}. \tag{5}$$

The surface dust input field is taken from the Global Ozone Chemistry Aerosol Radiation and

Transport (GOCART) model simulations [27]. The GOCART model assumes that all topographic lows with exposed surfaces are potential dust sources as a function of surface wind speed and wetness. In the GOCART model, dust is advected by wind fields from the Goddard Earth Observing System Data Assimilation System.

The surface export fields for POC, carbonate, biogenic opal flux and dust used to force the model are shown in Fig. 1.

The particulate mass (M_p) in g m^{-3} of seawater is given by the particle flux, F_p, in mol C m^{-2} yr^{-1}, the settling velocity, w_s, and the molar mass, J, so that $M_p = JF_p/w_s$. We follow Henderson et al. [9] and Marchal et al. [27] who used exponential penetration profiles to parameterise dissolution of $CaCO_3$ [28]

$$M_{car}(z) = M_{car}(z_0)\exp\left(\frac{z_0 - z}{z_p}\right), \quad (6)$$

where z is depth, z_0 the thickness of the euphotic zone, z_p is the penetration depth. (A summary of the values and symbols for the constants used in this paper is given in Table 1.)

Henderson et al. [9] also applied exponential dissolution profiles to biogenic opal. The behaviour of opal in the Southern Ocean is likely to be a significant factor in the distribution of ^{231}Pa and ^{230}Th there [7]. Here we use an alternative dissolution scheme to Henderson et al. [9], which is temperature dependent so that

$$D_{opal} = B(T - T_0), \quad (7)$$

where D_{opal} is the rate of biogenic opal dissolution in mol yr^{-1} and T is the water temperature at a given point in the model [29–31], T_0 is the minimum temperature of sea water in the model (−2 °C) and B is a constant set at 0.12 mol $°C^{-1}$ yr^{-1}. Temperature dependent opal dissolution leads to realistic, almost uniform vertical profiles of opal concentration in the Southern Ocean (e.g., [25]).

Dissolution of POC with respect to depth is described by a power law with exponent ε [32]

$$M_{POC}(z) = M_{POC}(z_0)\left(\frac{z}{z_0}\right)^{-\varepsilon}. \quad (8)$$

Values used for ε are given in Table 1.

An assumption of no dust dissolution is applied so that the dust concentration remains constant with depth.

Boundary scavenging refers to the range of processes by which nuclides are preferentially removed from the oceans at ocean margins and includes both the effect of high particle flux and particle type [33,34]— high lithogenic flux from rivers and coastal erosion provide an important primary source of particulate flux for scavenging while the supply of nutrients from rivers increases primary productivity which also increases the particulate flux available for scavenging close to the coasts. High productivity areas at the coast are resolved by the model in the form of upwelling zones but there is no representation of the input of lithogenic material at the coast. This means that boundary scavenging is represented in the model only by the effect of higher productivity in grid boxes close to the coast. The potential effect of nepheloid layers on the ^{231}Pa and ^{230}Th is not considered here other than that the sediment ^{231}Pa/^{230}Th is equilibrated with the water immediately above it.

2.3. Equilibrium partition coefficient scavenging model

We vary the K_p^i values for ^{231}Pa and ^{230}Th on biogenic opal, $CaCO_3$, POC and the dust flux according to the observations of Luo and Ku [11] and Chase et al. [10]. The activities of ^{231}Pa and ^{230}Th, in dissolved, A_d^i, and bulk particle-associated, A_b^i, form in dpm m^{-3} are calculated using Eqs. (9) and (10).

$$\frac{\partial A^i_{total}}{\partial t} = \beta^i - \lambda^i A^i_{total} - w_s \frac{\partial A^i_b}{\partial z} + Transport\left(A^i_{total}\right); \quad (9)$$

β is the production of new ^{231}Pa or ^{230}Th from the decay of ^{235}U and ^{234}U and λ is the radiodecay constant. The transport term represents the action of diffusion, convection and advection on the tracer movement and is provided by the Bern3D ocean model. The total activity of each isotope is advected in the model so that both particulate and dissolved forms advect. The total activity, A^i_{total}, is separated into the total or bulk particle-associated, A^i_b, and

dissolved, A^{i}_{d}, fractions by rearranging Eq. (1) for opal, POC, $CaCO_3$ and dust and summing the resulting terms:

$$\begin{aligned} A^{i}_{total} &= A^{i}_{b} + A^{i}_{d} \\ &= \left(K^{i}_{dust}C_{dust} + K^{i}_{POC}C_{POC} + K^{i}_{car}C_{car} \right. \\ &\quad \left. + K^{i}_{opal}C_{opal} + 1\right)A^{i}_{d} \end{aligned}$$

so that

$$A^{i}_{d} = \frac{A^{i}_{total}}{\left(K^{i}_{dust}C_{dust} + K^{i}_{POC}C_{POC} + K^{i}_{car}C_{car} + K^{i}_{opal}C_{opal} + 1\right)}. \quad (10)$$

Henderson et al. [9] assumed an inverse power-law dependence of K with respect to the particle concentration obtained by linear regression [4]. Such a relationship between K and particle concentration may be due to the complicated relationship between particle concentration and particle aggregation/settling [4] and is only apparent if shallow water data (with extremely high particle concentrations) are included. Chase et al. [10] argue that the particle concentration may also vary with the particle type and it is hard to distinguish in field data between the effects of particle type and particle concentration on the bulk sediment K values. It is uncertain whether the particle concentration effect on K is important in the deep ocean so we take the simplest approach and assume a constant K value with respect to particle concentration.

Chase et al. [10] suggest that the particle concentration effects may be due to scavenging disequilibria on rapidly falling particles for example during high production bloom events. Because we are interested in relatively long time-scale processes over the global ocean we force the model with annually averaged production fields and such a seasonal 'bloom effect' will not affect our results.

In order to consider the relative equilibrium partition coefficients of various particle types a reference equilibrium partition coefficient K_{ref} is defined. All other K values used in the model are stated as fractions of K_{ref} (Table 1). The ^{231}Pa and ^{230}Th distributions are assumed to have reached equilibrium when the ratio of the total ^{231}Pa activity to the total ^{230}Th activity reaching the sediment is equal to the production ratio of 0.093. The modelled 'sediment' ^{231}Pa and ^{230}Th activities are equivalent to the particulate ^{231}Pa and ^{230}Th in the deepest grid cells.

Sensitivity tests are carried out for variation in the particle settling velocity (w_s), K values and particle dissolution. The fractionation of ^{231}Pa and ^{230}Th by dust, $CaCO_3$, opal and POC is varied as a means to resolve the disagreement over the relative importance of these particle types in ocean ^{231}Pa/^{230}Th fractionation which exists in the literature [10–14].

2.4. A note on the vertical distribution of isotopes at steady state and the effects of transport and mixing

For steady state, and neglecting the effects of advection, diffusion and convection the effects of production, decay and settling must balance at any point in the ocean and Eq. (9) implies that

$$\beta^{i} - \lambda^{i}A^{i}_{total} - w_s\frac{\partial A^{i}_{b}}{\partial_z} = 0. \quad (11)$$

For typical values of A^{Th}_{total} and A^{Pa}_{total} the isotope decay term is three orders of magnitude less than the production term and for the purposes of this illustration is neglected. Rearranging the remaining terms and assuming that A^{i}_{b} at the surface is zero gives

$$A^{i}_{b}(z) = \frac{\beta^{i}}{w_s}\cdot z. \quad (12)$$

In other words the particle-associated isotope activities are expected to increase linearly with depth in agreement with observations [2,5]. The increase of particle-associated isotope activities with depth depends on the ratio β^{i}/w_s. Interestingly A^{i}_{b} is independent of the particle concentration. Because w_s is assumed to be the same for both ^{231}Pa and ^{230}Th the production ratio, $\beta^{Pa}/\beta^{Th}=0.093$, determines the ^{231}Pa/^{230}Th activity ratio at all points in the water column. Combining Eqs. (1) and (12) and noting that $C_i = F_i/\rho w_s$, where ρ is the fluid density, gives A^{i}_{d} as

$$A^{i}_{d}(z) = \frac{\rho\beta^{i}}{K^{i}_{b}F_{b}}\cdot z, \quad (13)$$

so that the dissolved activity of the isotopes is independent of w_s, remembering that the transport term has been neglected for the purposes of this analysis. In other words, it is the flux of particles which controls

the dissolved concentrations, not the rate at which they settle. As previously noted preferential transport of ^{231}Pa means that the ^{231}Pa/^{230}Th activity ratio in the ocean differs strongly from the production ratio and the relationship outlined in Eq. (11) shows that an additional source of A_d^i (i.e., the transport term) would affect A_b^i.

Ocean advection and diffusion distribute the isotopes in distinctly different ways. Diffusive transport moves the isotopes downgradient. Because the isotopes are removed by particles in areas of high particle flux these areas show reduced dissolved isotope concentrations. As a consequence of such reduced dissolved isotope concentrations there is a diffusive flux of dissolved isotopes into these areas and subsequent removal to the sediment. Diffusive transport of isotopes therefore increases the removal of ^{231}Pa and ^{230}Th in areas of high particle flux. Because ^{231}Pa has a longer residence time in the water column than ^{230}Th this process favours ^{231}Pa transport and areas of high particle flux have increased $^{231}Pa_{xs}/^{230}Th_{xs}$ ratios. Here we refer to this as the 'particle-flux mechanism' for generating high sediment $^{231}Pa_{xs}/^{230}Th_{xs}$. The advection of isotopes also preferentially transports ^{231}Pa but, unlike diffusive transport, advection transports tracers along the large-scale flow direction, which may be up or down the gradient of isotope concentration.

3. Results and discussion

3.1. Control run — Chase et al. [10] K values

The control run (Fig. 2) uses the values in Table 1 with K values taken from Chase et al. [10]. The ocean sediment ^{231}Pa/^{230}Th activity ratios are shown normalised to the production ratio (0.093) and on a $\log_{10}$ scale (Fig. 2). Many of the general features seen in observations are simulated by the control run. Both ^{231}Pa and ^{230}Th increase approximately linearly with respect to depth. Exceptions to the increase in isotope activity with depth exist in areas of deep-water formation where low values of ^{231}Pa and ^{230}Th activities are transported quickly from the surface to the deep ocean. Convection strongly reduces, or even reverses the process of accumulation of isotope activity with depth [35–37] and this is simulated by the model. In the case of particle-associated ^{230}Th and ^{231}Pa these depth-increases are most intense in the south Atlantic and Southern Ocean.

The Southern Ocean maximum in the sediment ^{231}Pa/^{230}Th activity ratio is well reproduced, as are the high values of ^{231}Pa/^{230}Th in the eastern equatorial Pacific. This southern ocean maximum is due to the efficient removal of ^{231}Pa in the southern ocean by the high opal flux there. ^{231}Pa is effectively transported to the southern ocean from the major ocean basins by the meridional overturning circulation [47]. Another contributing factor to the Southern Ocean ^{231}Pa sink is the southward shoaling of isopycnals within the Antarctic Circumpolar Current. This brings deep water with relatively high ^{231}Pa concentration to shallower depths where the equilibrium concentration is lower with respect to particle scavenging, thereby promoting adsorption [66]. There is also a maximum in the North Pacific corresponding to the region of high opal production there (Fig. 1). As suggested by Yu et al. [6] high productivity areas in the Atlantic have less effect on sediment ^{231}Pa/^{230}Th activity ratios than in the Pacific or Indian Oceans due to the relatively short residence time of deep water in the Atlantic.

Ocean sediment ^{231}Pa/^{230}Th activity ratios are lower in the oligotrophic gyre regions than in regions of high productivity due to the particle-flux effect. The modelled sediment ^{231}Pa/^{230}Th activity ratios in the ocean gyre regions are generally slightly higher than observed. The offset may be explained by the relatively low half life of ^{231}Pa compared to ^{230}Th. Given a 10 cm bioturbated sediment mixed layer and an accumulation rate of ~0.5 cm ka^{-1} surface sediments in the Pacific gyres might be as old as 20 ka so that the observed sediment surface ^{231}Pa will be considerably reduced compared to ^{230}Th.

Western north Atlantic cores are likely to be more sensitive to changes in the AMOC than those to the east due to the presence of the Deep Western Boundary Current (DWBC). This sensitivity gradient across the Atlantic is likely to be accentuated by the presence of higher particle flux regions to the eastern North Atlantic.

It is possible that the increase in the ^{231}Pa/^{230}Th activity ratio observed by McManus et al. [8] during H1 and discussed earlier in the text is the result of varying production in the region around the core site, though not at the site itself — in this way the core site

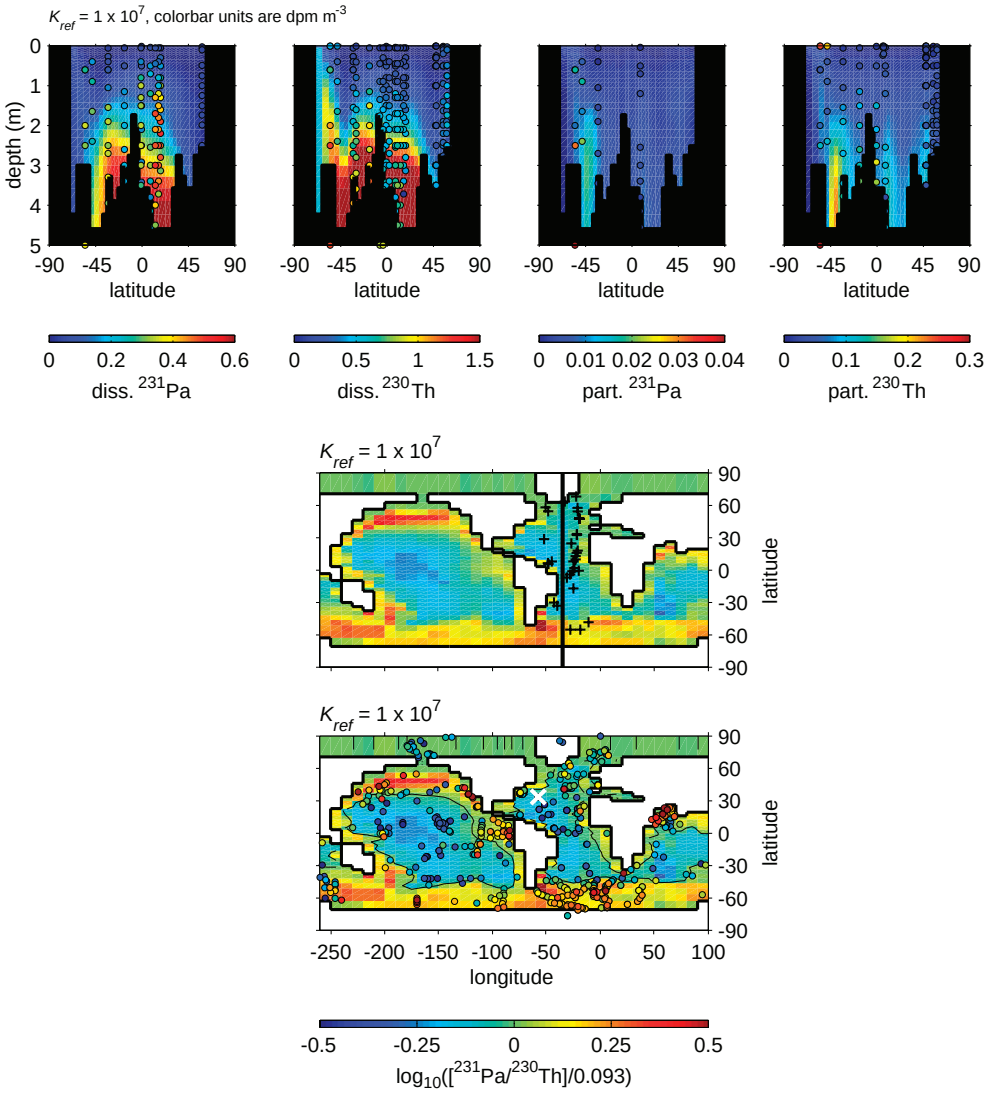

Fig. 2. Atlantic transects of dissolved and particle-associated ^{231}Pa and ^{230}Th (upper panels) and global sediment ^{231}Pa/^{230}Th activity ratios (lower panels). Parameter values in all panels are as for the 'control run' — relative K values are after Chase et al. [10] (Table 1). Coloured circles represent observations from Table 2. The crosses in the upper global plot represent the sites of the observations shown in the upper transects. The transects are taken along the black line shown in the upper global plot. The white cross on the lower global plot is the site of the core used in McManus [8]. Note that in the lower panels the ^{231}Pa/^{230}Th activity ratio is plotted relative to the production ratio (0.093) on a $\log_{10}$ scale. The contour line represents zero on the colour scale or ^{231}Pa/^{230}Th=0.093. The model parameters for the control run are z_p=2000 m, ε=0.858, w_s=1000 m yr^{-1}, $K_{ref}=1\times10^7$, $K^{Th}_{car}=K_{ref}$, $K^{Th}_{opal}=K_{ref}/20$, $K^{Th}_{POC}=K_{ref}$, $K^{Th}_{dust}=0$, $K^{Pa}_{car}=K_{ref}/40$, $K^{Pa}_{opal}=K_{ref}/6$, $K^{Pa}_{POC}=K_{ref}$, $K^{Pa}_{dust}=0$.

could have become part of a frontal region between areas of high and low ^{231}Pa/^{230}Th leaving no corresponding productivity signal in the core. It is important to consider multiple North Atlantic cores in order to tackle this issue.

The simulation of these general features of the ocean ^{231}Pa and ^{230}Th distribution is a first indication that the K values suggested by Chase et al. [10] are consistent with the ^{231}Pa and ^{230}Th scavenging model used here. Note that the simulation of the ocean ^{231}Pa

Table 2
References for data used in Figs. 2–8

Atlantic water column ^{231}Pa and ^{230}Th data	Global Holocene sediment $\frac{^{231}Pa_{xs}}{^{230}Th_{xs}}$
Colley et al., 1995 [39].	Anderson et al., 1983 [43].
Mangini and Key, 1983 [40].	Anderson et al., 1990 [34].
Moran et al., 1997 [35].	Anderson et al., 1994 [44].
Moran et al., 2001 [41].	Asmus et al. 1999 [45].
Rutgers van der Loeff and Berger, 1993 [42].	Bacon and Rosholt, 1982 [46].
Vogler et al., 1998 [37].	Chase et al. 2003 [47].
Walter et al. 1997 [38].	DeMaster, 1979 [48].
François R., unpublished data	Francois et al., 1993 [49].
	Frank et al., 1994 [50].
	Frank, 1996 [51].
	Ku et al., 1972 [52].
	Kumar, 1994 [53].
	Lao et al. 1992 [54].
	Mangini and Diester-Haas, 1983 [55].
	Mangini and Sonntag, 1977 [56].
	Mangini and Kuehnel, 1987 [57].
	Muller and Mangini, 1980 [58].
	Shimmield et al., 1986 [59].
	Shimmield and Price, 1988 [60].
	Schmitz et al., 1986 [61].
	Scholten et al., 1995 [62].
	Scholten et al. 2005 [63].
	Walter et al., 1997 [38].
	Yang et al., 1995 [64].
	Yang et al., 1986 [65].
	Yu et al., 1996 [6].
	Thomas A., Henderson G.M., McCave I.N. unpublished data

The xs subscript is used to indicate that the values are for excess ^{231} Pa and ^{230} Th which have been corrected for ^{231} Pa and ^{230} Th isotopes supported by U decay within the sediment and for post-deposition radiodecay.

and ^{230}Th distribution is possible without strong fractionation by lithogenic particles (in the control run K_{dust}^{Th} and K_{dust}^{Pa} are set to zero). The reproduction of various features of the ocean ^{231}Pa and ^{230}Th distribution by the control run brings into question the validity of the Luo and Ku [11] assertion that lithogenic particles are important scavengers of ^{231}Pa and ^{230}Th.

In preventing any isotope scavenging by dust in the control run we have shown that scavenging by dust does not dominate the global ^{231}Pa/^{230}Th distribution. We have avoided using model tuning to find an estimate for K_{dust}^{Pa} and K_{dust}^{Th}. There is a regional discrepancy between modelled and observed dissolved ^{230}Th concentrations in the North Atlantic. This discrepancy occurs in the region of the Saharan dust plume and might be explained by the scavenging of ^{230}Th by the significant dust flux in this region. This effect is in a limited region of the ocean and does not affect the results presented here but it is a first indication that dust may preferentially scavenge ^{230}Th compared to ^{231}Pa.

3.2. Sensitivity experiments

The effect of increasing K_{ref} but keeping the relationship between the various K values as for the control run (Table 1) is to adsorb more of the ^{231}Pa and ^{230}Th onto particles. The particles quickly remove this increased ^{231}Pa and ^{230}Th load to the sediment so that the transport of dissolved ^{231}Pa relative to ^{230}Th is reduced. At any one site ^{231}Pa and ^{230}Th are removed at a rate closer to their production ratio. This effect is seen in the plots for $K_{ref}=1\times10^{8}$, ten times the K_{ref} in the control run (Fig. 3). Preferential scavenging of ^{231}Pa does

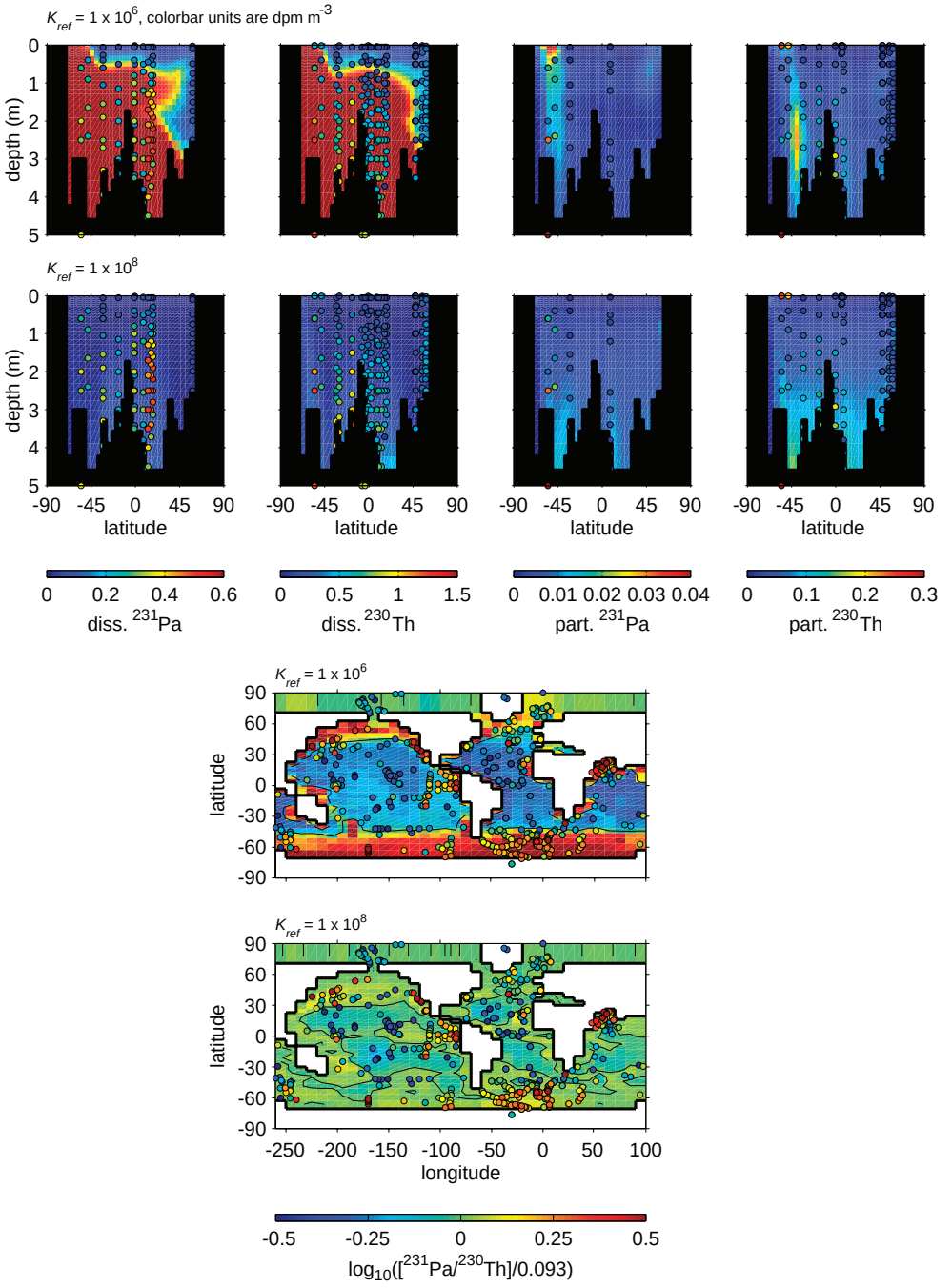

Fig. 3. Atlantic transects of dissolved and particle-associated ^{231}Pa and ^{230}Th (upper panels) and global sediment ^{231}Pa/^{230}Th activity ratios (lower panels). K_{ref} is varied between 1×10^6 and 1×10^8 for the two simulations shown. Coloured circles represent observations from Table 2. The transects are taken along the black line shown in Fig. 2. Note that in the lower panels the ^{231}Pa/^{230}Th activity ratio is plotted relative to the production ratio (0.093) on a $\log_{10}$ scale. The contour line represents zero on the colour scale or ^{231}Pa/^{230}Th=0.093. The model parameters which are constant for the two runs shown are z_p=2000 m, ε=0.858, w_s=1000 m yr^{-1}, $K^{Th}_{car}=K_{ref}$, $K^{Th}_{opal}=K_{ref}$ / 20, $K^{Th}_{POC}=K_{ref}$, K^{Th}_{dust}=0, $K^{Pa}_{car}=K_{ref}/40$, $K^{Pa}_{opal}=K_{ref}/6$, $K^{Pa}_{POC}=K_{ref}$, K^{Pa}_{dust}=0.

still occur for $K_{ref}=1\times10^8$ but it is much reduced and the global range of ^{231}Pa and^{230}Th in both the water column and sediments is much lower. The reverse is true if $K_{ref}=1\times10^6$ and the intensified transport of dissolved ^{231}Pa relative to ^{230}Th increases the global range of ^{231}Pa/^{230}Th activity ratios considerably. The two extreme cases represented in Fig. 3 suggest that the $K_{ref}=1\times10^7$, as used in the control run and found by Chase et al. [10], is the correct order of magnitude. A lower K_{ref} would improve the representation of the ocean gyres but it would result in too large an increase in ^{231}Pa/^{230}Th activity ratios in the Southern Ocean sediment.

Varying the exponent for POC dissolution, ε, in Eq. (8) varies the dissolution of POC with respect to depth. Higher values of ε give lower POC concentrations at depth due to increased dissolution. The POC fractionation ratio, $K_{POC}^{Th}/K_{POC}^{Pa}$, is 1 in the model so the results shown in Fig. 4 are straightforward to interpret. With lower POC flux the scavenging of ^{231}Pa is reduced, extending the residence time of the isotope in the water column. Note that the residence time of ^{230}Th is such that it does not demonstrate strong transport effects for the control run — the effect of further reduction of the ^{230}Th residence time is therefore not strongly visible in Fig. 4. There is generally more transport of ^{231}Pa compared to ^{230}Th which increases the range of sediment ^{231}Pa/^{230}Th activity ratios.

Fig. 5 shows the effect of varying the penetration depth, z_p of $CaCO_3$ in Eq. (6) on the global ^{231}Pa and ^{230}Th distribution. A first glance at the plots of global sediment ^{231}Pa/^{230}Th is somewhat puzzling. Increasing z_p increases particle concentrations and should therefore enhance scavenging, reducing the residence time of ^{231}Pa and the transport effect. Such an argument suggests that for deep z_p values the model should give reduced range of sediment ^{231}Pa/^{230}Th activity ratios but the plots in Fig. 5 show the opposite to be the case. Consideration of the effect of varying z_p on the dissolved isotopes resolves the apparent discrepancy. $CaCO_3$ preferentially carries ^{230}Th rather than ^{231}Pa to the sediment with a fractionation ratio, $K_{car}^{Th}/K_{car}^{Pa}$, of 40 in our simulation. Varying the penetration depth of $CaCO_3$ therefore affects ^{230}Th more strongly than ^{231}Pa. For shallow z_p a high rate of dissolution with respect to falling $CaCO_3$ is responsible for high levels of dissolved ^{230}Th at depth Eq. (1). High levels of dissolved ^{230}Th increase the transport of ^{230}Th in the ocean so that the range of ^{231}Pa/^{230}Th activity ratios in the ocean is reduced. The reverse is true for deep z_p values.

Experiments varying the constant B in Eq. (7) for opal dissolution by $\pm$50% were carried out but had an insignificant effect on the result and therefore are not shown.

Fig. 6 shows the effect of varying the settling velocity on the isotope distributions. This is seen clearly in the particle-associated isotope activities, which show increased ^{231}Pa and ^{230}Th activities for reduced settling velocities. Reduced settling velocity increases the ^{231}Pa and ^{230}Th activities associated with particles and is explained by Eq. (12), as discussed earlier in the text. This effect gives a proportional increase for both ^{231}Pa and ^{230}Th and so has negligible impact on the sediment ^{231}Pa/^{230}Th activity ratios. As suggested by Eq. (13) the same change in the settling velocity has negligible impact on the dissolved ^{231}Pa and ^{230}Th activities the ocean transport remains the same for both runs.

An exception is the Southern Ocean where some change in the sediment ^{231}Pa/^{230}Th activity ratios for high and low settling velocities is discernable. This is because opal dissolution is described in the model as a dissolution rate Eq. (7). Increasing the settling velocity decreases the amount of time opal is in the water column and subject to dissolution and so opal concentrations are increased at depth. Because of the high fractionation factor of opal ($K_{opal}^{Pa}/K_{opal}^{Th}=20/6$), increased opal concentrations lead to increased sediment ^{231}Pa/^{230}Th activity ratios in the Southern Ocean for high settling velocity.

3.3. Lithogenic vs. biogenic fractionation

Having established that the model is capable of reproducing many of the features of the global ^{231}Pa/^{230}Th distribution it is interesting to consider whether the approach presented here can resolve the disagreement about whether the lithogenic [13,14] or biogenic particle [10,12] fraction dominates the ^{231}Pa and ^{230}Th distribution in the ocean. Two simulations have been carried out using the K values from Luo and Ku [11]. Luo and Ku [11] state that ^{231}Pa scavenging by opal may be impor-

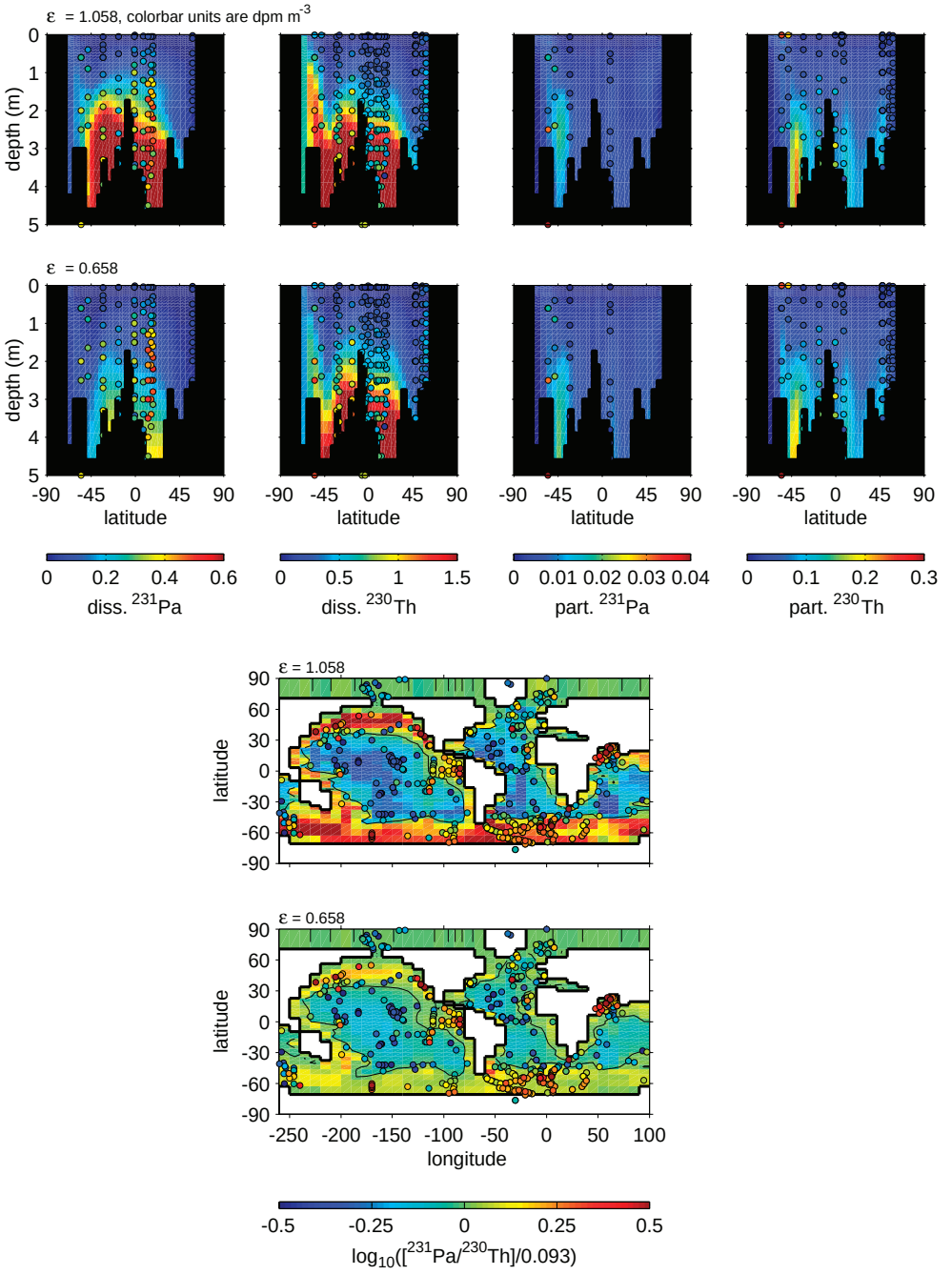

Fig. 4. Atlantic transects of dissolved and particle-associated ^{231}Pa and ^{230}Th (upper panel) and global sediment ^{231}Pa/^{230}Th activity ratios (lower panel). The exponent for POC dissolution, ε is varied between 1.058 and 0.658 for the two simulations shown. Coloured circles represent observations from Table 2. The transects are taken along the black line shown in Fig. 2. Note that in the lower panels the ^{231}Pa/^{230}Th activity ratio is plotted relative to the production ratio (0.093) on a $\log_{10}$ scale. The contour line represents zero on the colour scale or ^{231}Pa/^{230}Th=0.093. The model parameters which are constant for the two runs shown are z_p=2000 m, w_s=1000 m yr^{-1}, $K_{ref}=1\times10^7$, $K^{Th}_{car}=K_{ref}$, $K^{Th}_{opal}=K_{ref}/20$, $K^{Th}_{POC}=K_{ref}$, $K^{Th}_{dust}=0$, $K^{Pa}_{car}=K_{ref}/40$, $K^{Pa}_{opal}=K_{ref}/6$, $K^{Pa}_{POC}=K_{ref}$, $K^{Pa}_{dust}=0$.

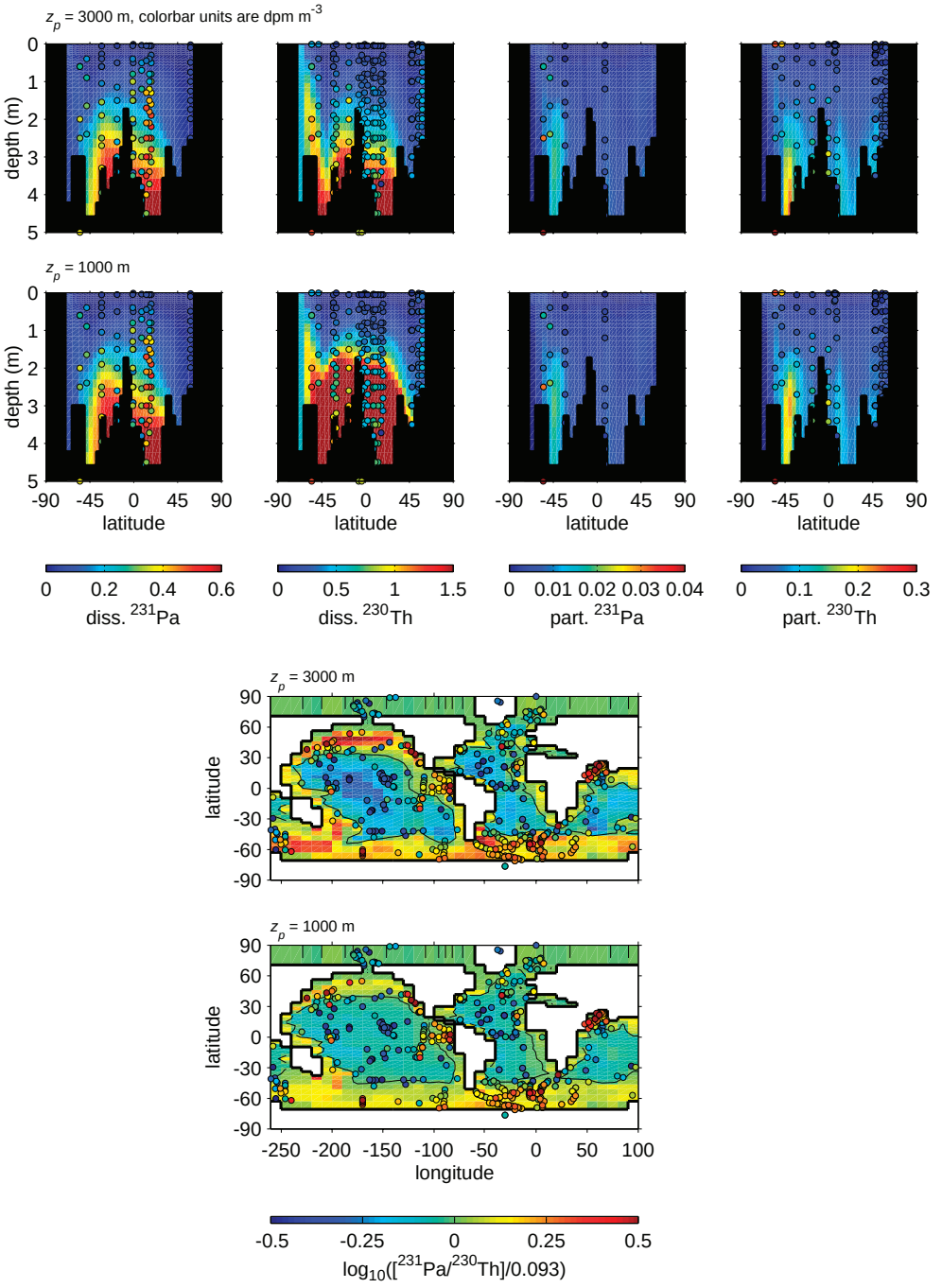

Fig. 5. Atlantic transects of dissolved and particle-associated ^{231}Pa and ^{230}Th (upper panels) and global sediment ^{231}Pa/^{230}Th activity ratios (lower panels). The penetration depth for $CaCO_3$, z_p, is varied between 3000 m and 1000 m for the two simulations shown. Coloured circles represent observations from Table 2. The transects are taken along the black line shown in Fig. 2. Note that in the lower panels the ^{231}Pa/^{230}Th activity ratio is plotted relative to the production ratio (0.093) on a $\log_{10}$ scale. The contour line represents zero on the colour scale or ^{231}Pa/^{230}Th=0.093. The model parameters which are constant for the two runs shown are ε=0.858, w_s=1000 m yr^{-1}, $K_{ref}=1\times10^7$, $K^{Th}_{car}=K_{ref}$, $K^{Th}_{opal}=K_{ref}/20$, $K^{Th}_{POC}=K_{ref}$, $K^{Th}_{dust}=0$, $K^{Pa}_{car}=K_{ref}/40$, $K^{Pa}_{opal}=K_{ref}/6$, $K^{Pa}_{POC}=K_{ref}$, $K^{Pa}_{dust}=0$.

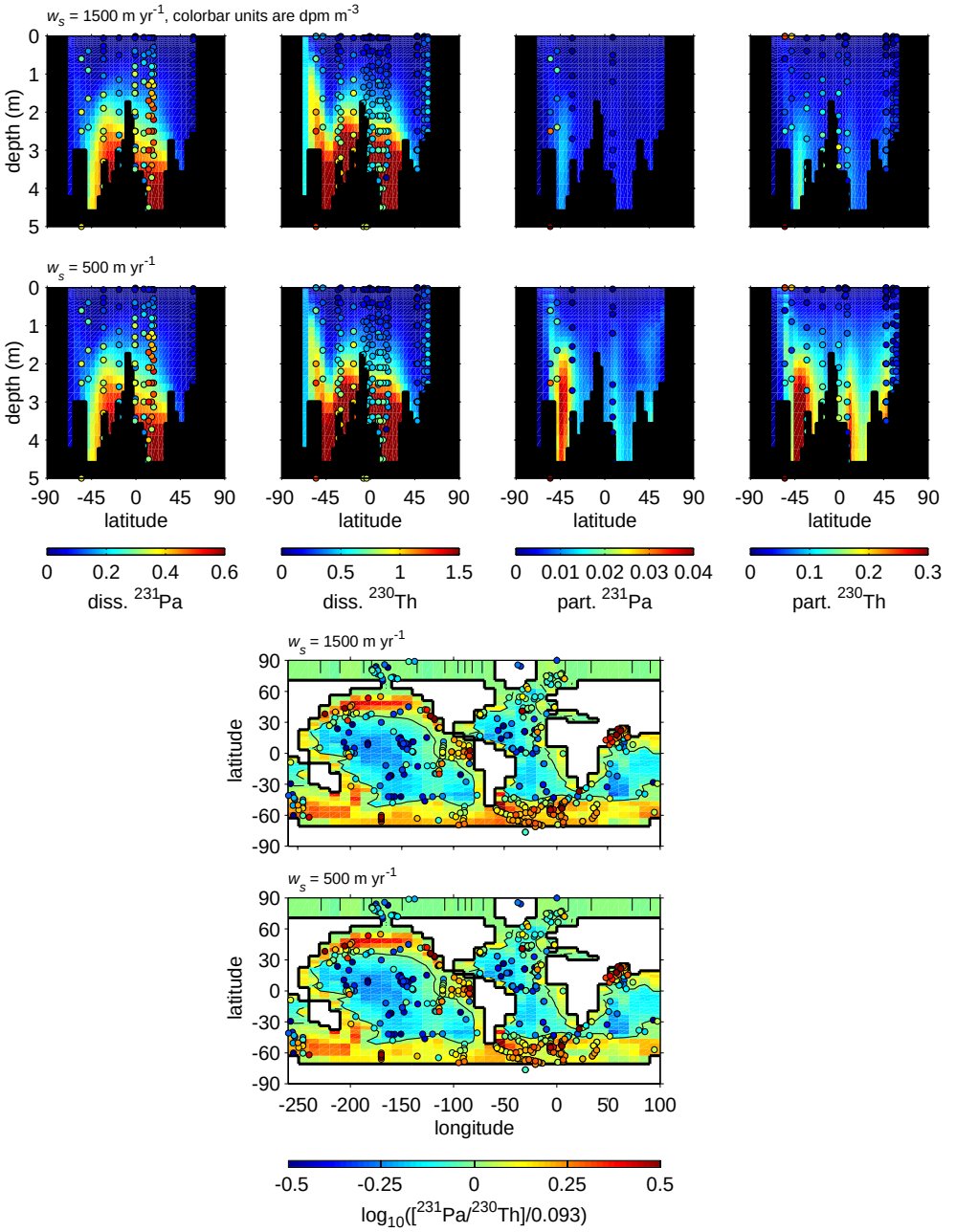

Fig. 6. Atlantic transects of dissolved and particle-associated ^{231}Pa and ^{230}Th (upper panels) and global sediment ^{231}Pa/^{230}Th activity ratios (lower panels). Settling velocities, w_s, are varied between 500 and 1500 m s^{-1}. Coloured circles represent observations from Table 2. The transects are taken along the black line shown in Fig. 2. Note that in the lower panels the ^{231}Pa/^{230}Th activity ratio is plotted relative to the production ratio (0.093) on a log$_{10}$ scale. The contour line represents zero on the colour scale or ^{231}Pa/^{230}Th=0.093. The model parameters which are constant for the two runs shown are z_p=2000 m, ε=0.858, $K_{ref}=1\times10^7$, $K^{Th}_{car}=K_{ref}$, $K^{Th}_{opal}=K_{ref}/20$, $K^{Th}_{POC}=K_{ref}$, $K^{Th}_{dust}=0$, $K^{Pa}_{car}=K_{ref}/40$, $K^{Pa}_{opal}=K_{ref}/6$, $K^{Pa}_{POC}=K_{ref}$, $K^{Pa}_{dust}=0$.

tant in opal rich areas. In order to consider this issue two simulations were carried out for which the fractionation factor of opal, $K^{Pa}_{opal}/K^{Th}_{opal}$, was set to 1 and 10 with all other K values after Luo and Ku [11] (Table 1).

The two simulations are shown in Fig. 7 where $K^{Th}_{dust}=1\times10^8$, which compares to Luo and Ku's [11,13,14] estimate of $(2.2\pm0.9)\times10^8$. Simulations were carried out using different K^{Th}_{dust} values (1×10^7 to 1×10^9) as well as different variations on $K^{Pa}_{opal}/K^{Th}_{opal}$ (2 to 20) but were all very similar and so only two of these simulations are shown in Fig. 7. Both of the dust-scavenging simulations demonstrate a classic 'particle-flux effect' due to high dust flux into the North Atlantic and North Pacific. Although the $^{231}Pa/^{230}Th$ fractionation factor for dust, $K^{Pa}_{dust}/K^{Th}_{dust}$ is ~0.1 the high dust flux areas in the North Atlantic and North Pacific (Fig. 1) overcome this fractionation effect via the 'particle-flux mechanism' whereby ^{231}Pa is preferentially removed in areas with high particle flux. In the Saharan plume the dust makes up around 25% of the total particle flux in the model and drives the 'particle-flux mechanism' there. In fact, because Luo and Ku [11] find $K^{Pa}_{dust}/K^{Th}_{dust}$ ~0.1, a greater proportion of the total ^{231}Pa is in the dissolved phase than is the case for ^{230}Th for the simulations shown in Fig. 7 and the dissolved ^{231}Pa is preferentially transported to areas of high dust flux. The Luo and Ku [11] relative fractionation factors therefore imply very high sediment $^{231}Pa/^{230}Th$ activity ratios corresponding to high dust flux in the North Atlantic. This seems quite at odds with numerous observations in the North Atlantic shown in the figure.

In Fig. 7 the much reduced scavenging by biogenic particles found by Luo and Ku [11] prevents the simulation of the high $^{231}Pa/^{230}Th$ activity ratios in the eastern equatorial Pacific. High $^{231}Pa/^{230}Th$ activity ratios in the eastern equatorial Pacific were simulated by runs with $K^{Th}_{dust}=1\times10^9$ (not shown here), although this value is unrealistically large.

It is clear that the Luo and Ku [11] fractionation ratios are quite at odds with the observations in the context of these model results. Luo and Ku [11] state: 'In highly productive waters with abundant biogenic particles, ^{231}Pa and ^{230}Th are scavenged with similar efficiencies, whereas in oligotrophic gyres where dominant particles are clays, the scavenging efficiency of ^{231}Pa is 10 times smaller than that of ^{230}Th. It is this difference in scavenging efficiency that allows ^{231}Pa to be transported more readily than ^{230}Th from oligotrophic oceans to areas of high productivity.' This statement does not take into consideration the preferential removal of ^{231}Pa in areas of high absolute dust flux (such as the North Atlantic) as illustrated in Fig. 7. The Luo and Ku [11] extrapolation of unprecedented high equilibrium partition coefficients for lithogenics from bulk particle samples with only ~5% lithogenic material may be outside the range of validity of the extrapolation. Fig. 1 makes clear another problem in the Luo and Ku [11] statement given here. While it is true that the dominant particles preserved in the sediment are clays, the flux of particles from the surface and within the water column is dominated by the biogenic component.

3.4. Weak adsorption of ^{230}Th onto biogenic opal

Chase et al. [10] state: 'Where the particle flux is dominated by opal, as in the Southern Ocean, sinking particles essentially do not fractionate between Th, Pa and Be (i.e., $F(Th/Pa)$ and $F(Th/Be)$ both = 1). This is due not only to the strong affinity of opal for Pa and for Be, but also, to the weaker affinity of opal for Th, relative to other particle types.' (F is the fractionation factor, K^{Pa}_p/K^{Th}_p.) This is a new suggestion about the scavenging of Th^{230} by opal and so here we test the consistency of this suggestion with our model and with the other K values presented by Chase et al. [10]. Note that although previous work to Chase et al. [10] has found that opal strongly scavenges Pa^{231} ($K^{Pa}_{opal}/K^{Th}_{opal}$ ~1 [38]). Chase et al. [10] are the first to identify that opal weakly scavenges ^{230}Th in finding that $K^{Th}_{opal}=K^{Th}_{car}/20$. Here we consider this assertion.

Fig. 8 shows a run with high scavenging by opal for both ^{231}Pa and ^{230}Th ($K^{Pa}_{opal}=K^{Th}_{opal}=K^{Th}_{car}$, thus the opal fractionation factor is 1). The band of high sediment $^{231}Pa/^{230}Th$ activity ratios around Antarctica moves northward towards the band of high $CaCO_3$ and POC flux and away from the maximum in opal production (Fig. 1). It seems that in the Southern Ocean there is a sensitive balance between fractionation by the effect of variation in productivity (the particle-flux effect) and fractionation by opal. If only the scavenging of ^{231}Pa onto opal is reduced to the observed value of Chase et al. [10] and the weak scavenging of ^{230}Th by opal is still

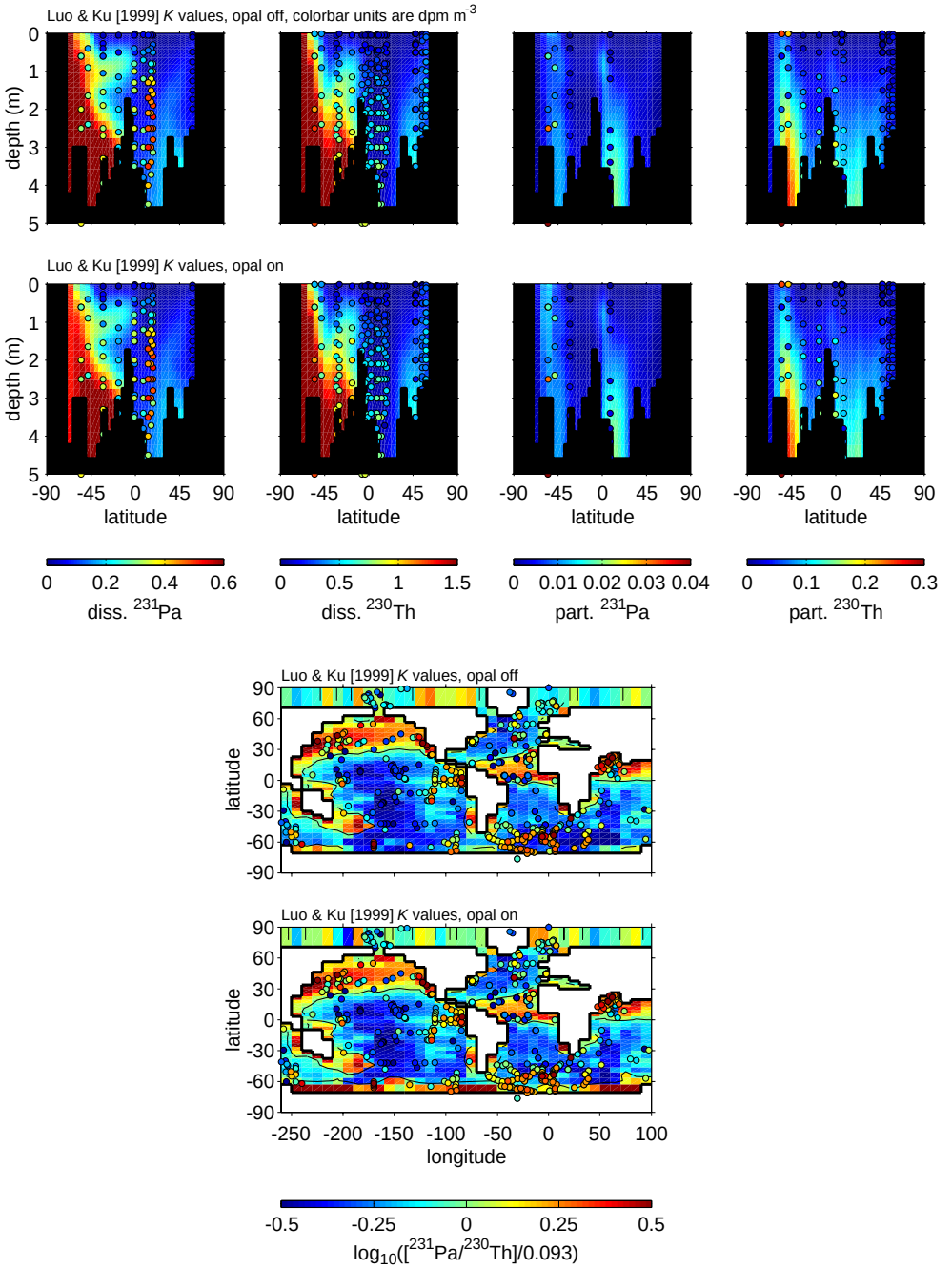

Fig. 7. Atlantic transects of dissolved and particle-associated ^{231}Pa and ^{230}Th (upper panels) and global sediment ^{231}Pa/^{230}Th activity ratios (lower panels). The K values are after Luo and Ku [11]. The two runs are with opal fractionation factors of 1 and 10, respectively. Coloured circles represent observations from Table 2. The transects are taken along the black line shown in Fig. 2. Note that in the lower panels the ^{231}Pa/^{230}Th activity ratio is plotted relative to the production ratio (0.093) on a $\log_{10}$ scale. The contour line represents zero on the colour scale or ^{231}Pa/^{230}Th=0.093. The model parameters which are constant for the two runs shown are z_p=2000 m, ε=0.858, w_s=1000 m yr^{-1}, $K_{\mathrm{ref}}=1\times10^7$, $K^{\mathrm{Th}}_{\mathrm{car}}=K_{\mathrm{ref}}/49$, $K^{\mathrm{Th}}_{\mathrm{opal}}=K_{\mathrm{ref}}/49$, $K^{\mathrm{Th}}_{\mathrm{POC}}=K_{\mathrm{ref}}/49$, $K^{\mathrm{Th}}_{\mathrm{dust}}=10\times K_{\mathrm{ref}}$, $K^{\mathrm{Pa}}_{\mathrm{car}}=K_{\mathrm{ref}}/49$, $K^{\mathrm{Pa}}_{\mathrm{POC}}=K_{\mathrm{ref}}/49$, $K^{\mathrm{Pa}}_{\mathrm{dust}}=K_{\mathrm{ref}}$.

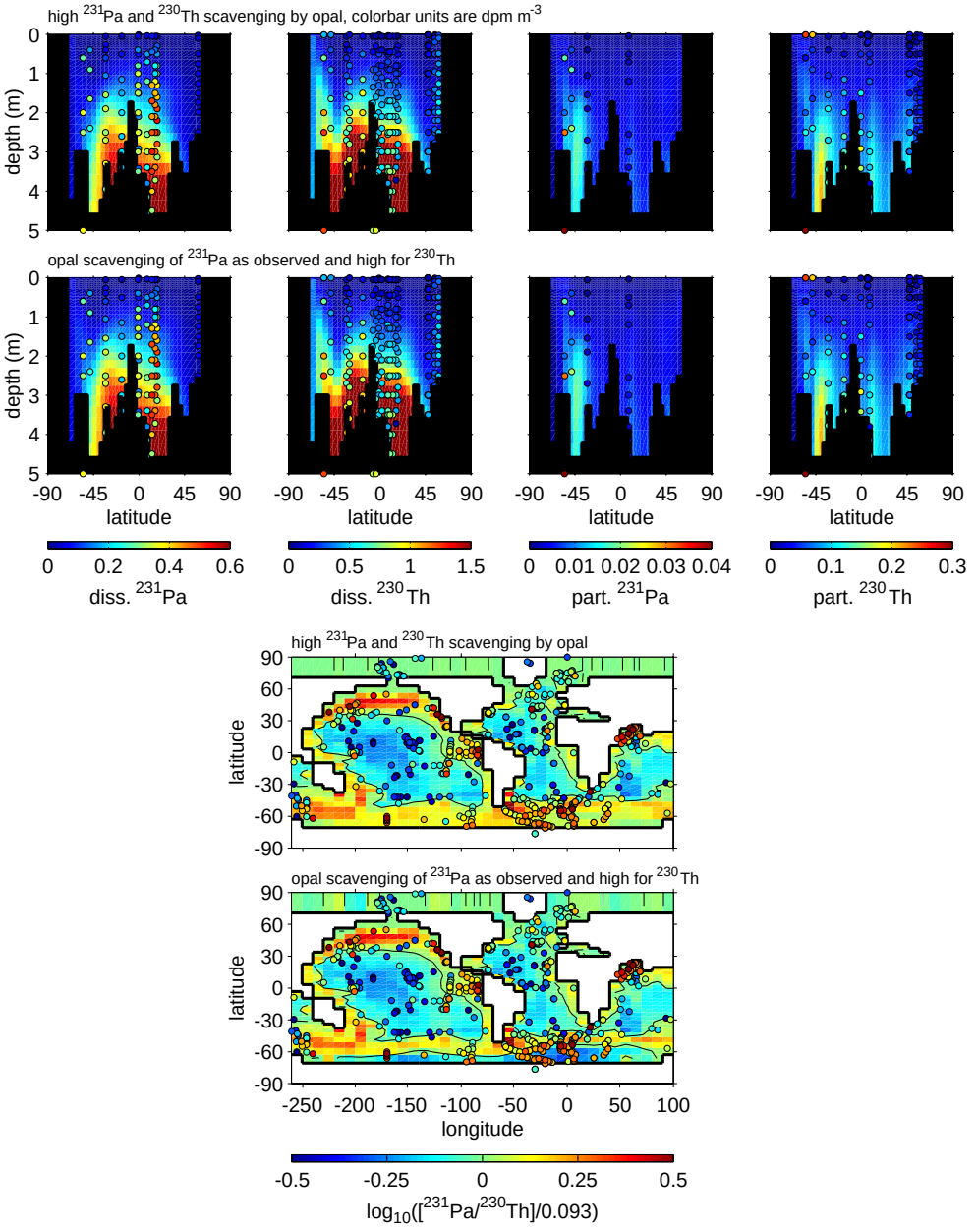

Fig. 8. Atlantic transects of dissolved and particle-associated ^{231}Pa and ^{230}Th (upper panels) and global sediment ^{231}Pa/^{230}Th activity ratios (lower panels). The relative K values test the assertion of Chase et al. [10] that opal weakly scavenges ^{230}Th. The simulation in the upper of each set of plots is from a run with equilibrium partition coefficients onto opal for both ^{231}Pa and ^{230}Th the same as for ^{230}Th onto $CaCO_3$ ($K^{Pa}_{opal}=K_{opal}{}^{Th}=K_{car}{}^{Th}$). The lower plots show the results from a run when only the scavenging of ^{231}Pa onto opal is adjusted to the observed value of Chase et al. [10] but the weak scavenging of ^{230}Th they observe is ignored ($K^{Pa}_{opal}=K^{Th}_{opal}/6=K^{Th}_{car}/6$). Coloured circles represent observations from Table 2. The transects are taken along the black line shown in Fig. 2. Note that in the lower panels the ^{231}Pa/^{230}Th activity ratio is plotted relative to the production ratio (0.093) on a $\log_{10}$ scale. The contour line represents zero on the colour scale or ^{231}Pa/^{230}Th=0.093. The model parameters which are constant for the two runs shown are z_p=2000 m, ε= 0.858, w_s=1000 m yr^{-1}, $K_{ref}=1\times10^7$, $K^{Th}_{car}=K_{ref}$, $K^{Th}_{POC}=K_{ref}$, $K^{Th}_{dust}=0$, $K^{Pa}_{car}=K_{ref}/40$, $K^{Pa}_{POC}=K_{ref}$, $K^{Pa}_{dust}=0$.

ignored ($K^{Pa}_{opal}=K^{Th}_{opal}/6=K^{Th}_{car}/6$) this effect is accentuated further and sediment $^{231}Pa/^{230}Th$ activity ratios around Antarctica fall below the production ratio.

The two simulations illustrated in Fig. 8 indicate an important self-consistency in the Chase et al. [10] work. Chase et al. [10] suggest that the scavenging of ^{231}Pa onto opal is less than the scavenging of ^{230}Th onto $CaCO_3$ ($K^{Pa}_{opal} \sim K^{Th}_{car}/6$). In this case the model indicates that the scavenging of ^{230}Th onto opal must also be less than the scavenging of ^{230}Th onto $CaCO_3$ ($K^{Th}_{opal} < K^{Th}_{car}/6$) in order for our model to simulate the observed ^{231}Pa and ^{230}Th around Antarctica. Chase et al. [10] find $K^{Th}_{opal} \sim K^{Th}_{car}/20$, in good agreement with the model prediction. This work therefore provides an objective test of the Chase et al. [10] suggestion that opal is a poor scavenger of ^{230}Th— this is consistent with the other K values they present.

The observed Southern Ocean maximum in sediment $^{231}Pa_{xs}/^{230}Th_{xs}$ is simulated by the control run due both to the relatively high scavenging of ^{231}Pa by opal compared to $CaCO_3$, and weak scavenging of ^{230}Th by $CaCO_3$. High sediment $^{231}Pa/^{230}Th$ activity ratios in the Southern Ocean are therefore a product of fractionation by opal ($K^{Pa}_{opal}/K^{Th}_{opal} \sim 3$). This conclusion compares to that of Walter et al. [38] and Marchal et al. [7] who found $K^{Pa}_{opal}/K^{Th}_{opal} \sim 1$.

3.4.1. Concluding remarks

The ability to represent the modern global ^{231}Pa and ^{230}Th distribution using a simple scavenging model, which is sensitive to ocean circulation, particle flux and particle type makes the sediment $^{231}Pa_{xs}/^{230}Th_{xs}$ a potentially extremely useful paleo-proxy (see also Marchal et al. [7]). The success of this particular model at simulating realistic core-top sediment $^{231}Pa/^{230}Th$ distributions makes it a powerful tool with which to interpret down-core records of $^{231}Pa_{xs}/^{230}Th_{xs}$ in terms of ocean circulation and particle fluxes.

These results strongly favour the Chase et al. [10] K values over those of Luo and Ku [11]. The Chase et al. [10] K values are self-consistent and when implemented in the model presented here they effectively represent many aspects of the global ^{231}Pa and ^{230}Th distribution.

Future work on global ^{231}Pa and ^{230}Th might consider issues not addressed here. A clearer understanding of the effects of nepheloid layers on scavenging, the effects of the input of lithogenic material at the ocean margins and remineralisation within the sediment structure would make interesting avenues for future research.

Acknowledgements

Thanks to Roger François, Alex Thomas, and Nick McCave who provided unpublished ^{231}Pa and ^{230}Th data. Bob Anderson and Roger François provided insightful reviews. Mian Chin provided the results from the GOCART model for annual average dust deposition. Olivier Marchal and Jerry McManus have provided useful discussion. Funding was made available from the STOPFEN European Network research project (HPRN-CT-2002-00221). Support from the Swiss National Science Foundation and the University of Bern is acknowledged.

References

[1] J.H. Chen, R.L. Edwards, G.J. Wasserburg, ^{238}U, ^{234}U and ^{232}Th in seawater, Earth Planet. Sci. Lett. 80 (1986) 241–251.
[2] M.P. Bacon, R.F. Anderson, Distribution of thorium isotopes between dissolved and particulate forms in the deep sea, J. Geophys. Res. 87 (1982) 2045–2056.
[3] Y. Nozaki, S.H. Yang, M. Yamada, Scavenging of thorium in the ocean, J. Geophys. Res. 92 (1987) 772–778.
[4] B.D. Honeyman, L.S. Balistrieri, J.W. Murray, Oceanic trace metal scavenging: the importance of particle concentration, Deep-Sea Res. 35 (1988) 227–246.
[5] M. Roy-Barman, J.H. Chen, G.J. Wasserburg, ^{230}Th–^{232}Th systematics in the central Pacific Ocean: the sources and fates of thorium, Earth Planet. Sci. Lett. 139 (1996) 351–363.
[6] E.F. Yu, R. Francois, M.P. Bacon, Similar rates of modern and last-glacial ocean thermohaline circulation inferred from radiochemical data, Nature 379 (1996) 689–694.
[7] O. Marchal, R. François, T.F. Stocker, F. Joos, Ocean thermohaline circulation and sedimentary $^{231}Pa/^{230}Th$ ratio, Paleoceanography 15 (2000) 625–641.
[8] J.F. McManus, R. Francois, J.-M. Gherardi, L.D. Keigwin, S. Brown-Leger, Collapse and rapid resumption of Atlantic meridional circulation linked to deglacial climate changes, Nature 428 (2004) 834–837.
[9] G.M. Henderson, C. Heinze, R.F. Anderson, A.M.E. Winguth, Global distribution of the ^{230}Th flux to ocean sediments constrained by GCM modelling, Deep-Sea Res. I 46 (1999) 1861–1894.
[10] Z. Chase, R.F. Anderson, M.Q. Fleisher, P.W. Kubik, The influence of particle composition and particle flux on scavenging of Th, Pa and Be in the ocean, Earth Planet. Sci. Lett. 204 (2002) 215–219.

[11] S. Luo, T.-L. Ku, Oceanic $^{231}Pa/^{230}Th$ ratio influenced by particle composition and remineralisation, Earth Planet. Sci. Lett. 167 (1999) 183–199.
[12] Z. Chase, R.F. Anderson, Comment on "On the importance of opal, carbonate, and lithogenic clays in scavenging and fractionating ^{230}Th, ^{231}Pa and ^{10}Be in the ocean" by S. Luo and T.-L. Ku, Earth Planet. Sci. Lett. 220 (2004) 213–222.
[13] S. Luo, T.-L. Ku, On the importance of opal, carbonate, and lithogenic clays in scavenging and fractionating ^{230}Th, ^{231}Pa and ^{10}Be in the ocean, Earth Planet. Sci. Lett. 220 (2004) 201–211.
[14] S. Luo, T.-L. Ku, Reply to Comment on "On the importance of opal, carbonate, and lithogenic clays in scavenging and fractionating ^{230}Th, ^{231}Pa and ^{10}Be in the ocean", Earth Planet. Sci. Lett. 220 (2004) 223–229.
[15] L. Guo, P.H. Santschi, M. Baskaran, A. Zindler, Distribution of dissolved and particulate ^{230}Th and ^{232}Th in seawater from the Gulf of Mexico and off Cape Hatteras as measured by SIMS, Earth Planet. Sci. Lett. 133 (1995) 117–128.
[16] S.A. Müller, F. Joos, N.R. Edwards, T.F. Stocker, Water mass distribution and ventilation time scales in a cost-efficient, 3-dimensional ocean model, J. Clim. (submitted for publication).
[17] N.R. Edwards, R. Marsh, Uncertainties due to transport-parameter sensitivity in an efficient 3-D ocean-climate model, Clim. Dyn. 24 (4) (2005) 415.
[18] S. Levitus, T. Boyer, World Ocean Atlas 1994 Volume 4: Temperature, NOAA Atlas NESDIS, U.S. Department of Commerce, Washington, D.C., 1994.
[19] NCEP Reanalysis data provided by the NOAA-CIRES Climate Diagnostics Center, Boulder, Colorado, USA, from their Web site at http://www.cdc.noaa.gov/.
[20] K. Matsumoto, J.L. Sarmiento, R.M. Key, O. Aumont, J.L. Bullister, K. Caldeira, J.-M. Campin, S.C. Doney, H. Drange, J.-C. Dutay, M. Follows, Y. Gao, A. Gnanadesikan, N. Gruber, A. Ishida, F. Joos, K. Lindsay, E. Maier-Reimer, J.C. Marshall, R.J. Matear, P. Monfray, R. Najjar, G.-K. Plattner, R. Schlitzer, R. Slater, P.S. Swathi, I.J. Totterdell, M.-F. Weirig, Y. Yamanaka, A. Yool, J.C. Orr, Evaluation of ocean carbon cycle models with data-based metrics, Geophys. Res. Lett. 31 (2004), doi:10.1029/2003GL018970.
[21] E.A. Laws, P.G. Falkowski, W.O. Smith Jr., H. Ducklow, J.J. McCarthy, Temperature effects on export production in the open ocean, Glob. Biogeochem. Cycles 14 (2000) 1231–1246.
[22] M.G. Behrenfeld, P.G. Falkowski, Photosynthetic rates derived from satellite-based chlorophyll concentration, Limnol. Oceanogr. 42 (1997) 1–20.
[23] E. Maier-Reimer, Geochemical cycles in an ocean general circulation model: preindustrial tracer distributions, Glob. Biogeochem. Cycles 7 (1993) 645–677.
[24] M. Conkright, S. Levitus, T. Boyer, World Ocean Atlas 1994 Volume 1: Nutrients, NOAA Atlas NESDIS, U.S. Department of Commerce, Washington, D.C., 1994.
[25] D.M. Nelson, L.I. Gordon, Production and pelagic dissolution of biogenic silica in the Southern Ocean, Geochim. Cosmochim. Acta 46 (1982) 491–501.
[26] C. Heinze, Zur Erniedrigung des Atmosphärischen Kohlendioxidgehalts durch den Weltozean während der letzen Eiszeit. Max-Planck-Inst. für Meteorol., Hamburg, Germany, Tech. Rep. 3 (1990) 1–180.
[27] P. Ginoux, M. Chin, I. Tegen, J. Prospero, B. Holben, O. Dubovik, S.-J. Lin, Sources and global distributions of dust aerosols simulated with the GOCART model, J. Geophys. Res. 106 (20) (2001) 255–273.
[28] J.H. Martin, G.A. Knauer, D.M. Karl, W.W. Broenkow, VERTEX: carbon cycling in the northeast Pacific, Deep-Sea Res. 34 (1987) 267–285.
[29] A. Kamatami, J.P. Riley, Rate of dissolution of diatom silica walls in seawater, Mar. Biol. 68 (1979) 91–96.
[31] P.A. Tréguer, S. Gueneley, B. Quéguiner, Kinetics of dissolution of Antarctic diatom frustules and the biogeochemical cycle of silicon in the Southern Ocean, Polar Biol. 9 (1989) 397–403.
[32] O. Marchal, T.F. Stocker, F. Joos, A latitude–depth, circulation-biogeochemical ocean model for paleoclimate studies. Development and sensitivities, Tellus 50 (1998) 290–316.
[33] M.P. Bacon, D.W. Spencer, P.G. Brewer, $^{210}Pb/^{226}Ra$ and $^{210}Po/^{210}Pb$ disequilibria in seawater and suspended particulate matter, Earth Planet. Sci. Lett. 32 (1976) 277–296.
[34] R.F. Anderson, Y. Lao, W.S. Broecker, S.E. Trumbore, H.J. Hofmann, W. Wolfi, Boundary scavenging in the Pacific Ocean: a comparison of ^{10}Be and ^{231}Pa, Earth Planet. Sci. Lett. 96 (1990) 287–304.
[35] S.B. Moran, M.A. Charette, J.A. Hoff, R.L. Edwards, W.M. Landing, Distribution of ^{230}Th in the Labrador Sea and its relation to ventilation, Earth Planet. Sci. Lett. 150 (1997) 151–160.
[36] S.B. Moran, C.-C. Shen, H.N. Edmonds, S.E. Weinstein, J.N. Smith, R.L. Edwards, Dissolved and particulate ^{231}Pa and ^{230}Th in the Atlantic Ocean: constraints on intermediate/deep water age, boundary scavenging, and $^{231}Pa/^{230}Th$ fractionation, Earth Planet. Sci. Lett. 203 (2002) 999–1014.
[37] S. Vogler, J. Scholten, M. Rutgers van der Loeff, A. Mangini, ^{230}Th in the eastern North Atlantic: the importance of water mass ventilation in the balance of ^{230}Th, Earth Planet. Sci. Lett. 156 (1998) 61–74.
[38] H.J. Walter, M.M. Rutgers van der Loeff, H. Hoeltzen, Enhanced scavenging of ^{231}Pa relative to ^{230}Th in the South Atlantic south of the Polar Front: implications for the use of the $^{231}Pa/^{230}Th$ ratio as a paleoproductivity proxy, Earth Planet. Sci. Lett. 149 (1997) 85–100.
[39] S. Colley, J. Thomson, P.P. Newton, Detailed ^{230}Th, ^{232}Th and ^{210}Pb fluxes recorded by the 1989/90 BOFS sediment trap time-series at 48°N, 20°W, Deep-Sea Res. 42 (6) (1995) 833–848.
[40] A. Mangini, R.M. Key, A ^{230}Th profile in the Atlantic ocean, Earth Planet. Sci. Lett. 62 (1983) 377–384.
[41] S.B. Moran, C.-C. Shen, S.E. Weinstein, L.H. Hettinger, J.H. Hoff, H.N. Edmonds, R.L. Edwards, Constraints on deep water age and particle flux in the equatorial and Southern Atlantic ocean based on seawater ^{231}Pa and ^{230}Th data, Geophys. Res. Lett. 28 (18) (2001) 3437–3440.
[42] M.M. Rutgers van der Loeff, G.W. Berger, Scavenging of ^{230}Th and ^{231}Pa near the Antarctic Polar Front in the South Atlantic, Deep-Sea Res. I 40 (1993) 339–357.

[43] R.F. Anderson, M.P. Bacon, P.G. Brewer, Removal of ^{230}Th and ^{231}Pa from the open ocean, Earth Planet. Sci. Lett. 62 (1983) 7–23.

[44] R.F. Anderson, M.Q. Fleisher, P.E. Biscaye, N. Kumar, B. Dittrich, P. Kubik, M. Suter, Anomolous boundary scavenging in the Middle Atlantic Bight: evidence from ^{230}Th, ^{231}Pa, ^{10}Be and ^{210}Pb, Deep-Sea Res. 41 (2/3) (1994) 537–561.

[45] T. Asmus, M. Frank, C. Koschmieder, N. Frank, R. Gersonde, G. Kuhn, A. Mangini, Variations of biogenic particle flux in the southern Atlantic section of the Subantarctic Zone during the Late Quaternary: evidence from $^{231}Pa_{ex}$ and $^{230}Th_{ex}$, Mar. Geol. 159 (1999) 63–78.

[46] M.P. Bacon, J.N. Rosholt, Accumulation rates of ^{230}Th, ^{231}Pa, and some transition metals on the Bermuda Rise, Geochim. Cosmochim. Acta 46 (1982) 651–666.

[47] Z. Chase, R.F. Anderson, M.Q. Fleisher, P. Kubik, Scavenging of ^{230}Th, ^{231}Pa and ^{10}Be in the Southern Ocean (SW Pacific sector): the importance of particle flux and advection, Deep-Sea Res. II 50 (2003) 739–768.

[48] D.J. DeMaster, The marine budgets of silica and ^{32}Si. Ph.D., Yale, 1979.

[49] R. Francois, M.P. Bacon, M.A. Altabet, Glacial/interglacial changes in sediment rain rate in the SW Indian sector of subantarctic waters as recorded by ^{230}Th, ^{231}Pa, U, and ^{d15}N, Paleoceanography 8 (5) (1993) 611–629.

[50] M. Frank, J.-D. Eckhardt, A. Eisenhauer, P.W. Kubik, B. Dittrich-Hannen, M. Segl, A. Mangini, Beryllium-10, thorium-230 and protactinium-231 in Galapagos microplate sediments: implications of hydrothermal activity and paleoproductivity changes during the last 100,000 years, Paleoceanography 9 (4) (1994) 559–578.

[51] M. Frank, Reconstruction of Late Quaternary environmental conditions applying the natural radionuclides ^{230}Th, ^{10}Be, ^{231}Pa and ^{238}U: a study of deep-sea sediments from the eastern sector of the Antarctic Circumpolar Current System, Ph.D., Alfred Wegener Institute for Polar and Marine Research (1996).

[52] T.-L. Ku, J.L. Bischoff, A. Boersma, Age studies of Mid-Atlantic Ridge sediments near 42°N and 20°N, Earth Planet. Sci. Lett. 19 (1972) 233–247.

[53] N. Kumar, Trace metals and natural radionuclides as tracers of ocean productivity. Ph.D., Columbia, 1994.

[54] Y. Lao, R.F. Anderson, W.S. Broecker, S.E. Trumbore, H.J. Hofmann, W. Wolfli, Transport and burial rates of ^{10}Be and ^{231}Pa in the Pacific Ocean during the Holocene period, Earth Planet. Sci. Lett. 113 (1992) 173–189.

[55] A. Mangini, L. Diester-Haas, Excess Th-230 in sediments off NW Africa traces upwelling during the past 130,000 years, in: E. Suess, J. Thiede (Eds.), Coastal Upwelling: Its Sedimentary Records, Plenum, 1983, pp. 455–470.

[56] A. Mangini, C. Sonntag, ^{231}Pa dating of deep-sea cores via ^{227}Th counting, Earth Planet. Sci. Lett. 37 (2) (1977) 251–256.

[57] A. Mangini, U. Kuehnel, Depositional history in the Clarion–Clipperton zone during the last 250,000 years; ^{230}Th and ^{231}Pa methods, Geol. Jahrb. 87 (1987) 105–121.

[58] P.J. Muller, A. Mangini, Organic carbon decomposition rates in sediments of the Pacific manganese nodule belt dated by ^{230}Th and ^{231}Pa, Earth Planet. Sci. Lett. 51 (1980) 94–114.

[59] G.B. Shimmield, J.W. Murray, J. Thomson, M.P. Bacon, R.F. Anderson, N.B. Price, The distribution and behaviour of ^{230}Th and ^{231}Pa at an ocean margin. Baja California, Mexico, Geochim. Cosmochim. Acta 50 (1986) 2499–2507.

[60] G.B. Shimmield, N.B. Price, The scavenging of U, ^{230}Th, and ^{231}Pa during pulsed hydrothermal activity at 20°S, East Pacific Rise, Geochim. Cosmochim. Acta 52 (1988) 669–677.

[61] W. Schmitz, A. Mangini, P. Stoffers, G.P. Glasby, W.L. Plueger, Sediment accumulation rates in the southwestern Pacific Basin and Aitutaki Passage, Mar. Geol. 73 (1–2) (1986) 181–190.

[62] J.C. Scholten, M.M. Rutgers van der Loeff, A. Michel, Distribution of ^{230}Th and ^{231}Pa in the water column in relation to the ventilation of the deep Arctic basins, Deep-Sea Res. 42 (6) (1995) 1519–1531.

[63] J.C. Scholten, J. Fietzke, A. Mangini, P. Stoffers, T. Rixen, B. Gaye-Haake, T. Blanz, V. Ramaswamy, F. Siroko, H. Schulz, V. Ittekkot, Radionuclide fluxes in the Arabian Sea: the role of particle composition, Earth Planet. Sci. Lett. 230 (3–4) (2005) 319–337.

[64] H.-S. Yang, Y. Nozaki, H. Sakai, A. Masuda, The distribution of ^{230}Th and ^{231}Pa in the deep-sea surface sediment of the Pacific Ocean, Geochim. Cosmochim. Acta 50 (1986) 81–89.

[65] Y.-L. Yang, H. Elderfield, T.F. Pedersen, M. Ivanovich, Geochemical record of the Panama basin during the last glacial maximum carbon event shows that the glacial ocean was not suboxic, Geology 23 (12) (1995) 1115–1118.

[66] R. Francois, M. Frank, M.M. Rutgers van der Loeff, M.P. Bacon, 230 Th normalization: an essential tool for interpreting sedimentary fluxes during the late Quaternary, Paleoceanography 19 (2004) A1018.